*Numerical Heat Transfer, Part B*, 57: 46–73, 2010

ISSN: 1040-7790 print/1521-0626 online
DOI: 10.1080/10407791003613702



# VERIFICATION OF MULTIDIMENSIONAL AND TRANSIENT CFD SOLUTIONS

**C. Orozco, D. Kızıldağ, A. Oliva, and C. D. Pérez-Segarra**
*Centre Tecnològic de Transferència de Calor (CTTC), Universitat Politècnica de Catalunya (UPC), Terrassa, Barcelona, Spain*

***This work addresses the verification of multidimensional and transient numerical solutions based on Richardson extrapolation techniques. Alternative extrapolation strategies based on both simultaneous (SCR) and independent (ICR) space-and-time coordinates refinement studies are investigated. Extrapolation strategies studied encompass the generalized Richardson extrapolation (GRE) based on both the local and the global observed order of accuracy, and the mixed-order Richardson extrapolation (MORE). Performance of all verification methods investigated has been tested on a manufactured solution and on the flows in different piston–cylinder configurations. Results reveal that the global observed order of accuracy and the postprocessing estimators obtained from ICR studies can provide useful information on which the most suitable verification methods can be selected.***

## 1. INTRODUCTION

The last decades have seen an important increase in the use of computational fluid dynamics (CFD) as an everyday tool to obtain solutions to many thermal and fluid dynamic problems. During this time, as both computers and numerical algorithms have become more efficient, CFD tools have systematically been applied to tackle a wider and wider range of problems of increasing complexity. However, despite the popularisation of these tools, CFD is still far from being a completely mature technology. The accuracy of the solutions provided by well-verified CFD codes depends to a great extent on the use of adequate mathematical models, computational meshes, and solvers which allow sufficient iterative convergence of the solutions. As a consequence, the credibility of the solutions provided by CFD tools and, therefore, its suitability in designing and optimization tasks, depends greatly on the correct development and use of these tools. This concern with the correct application of the CFD tools, and with the accuracy and the quantification of the uncertainties of the numerical solutions obtained, is addressed

Received 30 April 2009; accepted 28 December 2009.

This work has been financially supported by the Ministerio de Educación y Ciencia, Secretaría de Estado de Universidades e Investigación, Spain (ref. ENE2007-67185). The first and the second authors would also like to thank the financial support of Generalitat de Catalunya (ref. 2002 FI 00787 and ref. 2006 FI 01227).

Address correspondence to Assensi Oliva, Lab. Termotecnia I Energetica, Centre Tecnològic de Transferència de Calor (CTTC), Universitat Politècnica de Catalunya (UPC), ETSEIAT, C. Colom 11, 08222 Terrassa, Barcelona, Spain. E-mail: cttc@cttc.upc.edu

## NOMENCLATURE

| | | | |
|---|---|---|---|
| $C_i$ | $i$th-order error term coefficient | $t$ | time |
| $e_D$ | discretization error | $t_f$ | final time instant |
| $F_s$ | safety factor | $v_r$, $v_z$ | radial and axial components of velocity |
| GCI | grid convergence index | $V_p$ | piston velocity |
| $h$ | parameter representative of the grid spacing | $V_0$ | reference velocity |
| | | $\mathbf{x}$ | coordinates vector |
| MMS | method of manufactured solutions | $\varepsilon_{ij}$ | difference between solutions variables on grid levels $i$ and $j$ |
| $p$ | observed order of accuracy (equation(4)); pressure | $\sigma_p$ | standard deviation of $p$ |
| | | $\phi$ | solution variable |
| $p_r$ | value of $p$ that provides the exact discretization error (equation (8)) | $\phi_E$ | exact solution |
| | | $\phi_{\text{extr}}$ | extrapolated solution |
| $r$ | grid refinement ratio | | |
| $R_n$ | percentage of Richardson nodes | | |



by the validation and verification (V&V) discipline. Although initially developed by the operations research community [1], parallel to the popularization of CFD, V&V has received increasing attention by the CFD community. The terms *verification* and *validation* are used in this context to refer to "solving the equations right" and "solving the right equations," respectively [2]. Therefore, while validation is concerned with the modeling uncertainty, i.e., the errors associated with the mathematical model used in the modelization of the physics involved, verification is focused on the numerical uncertainty, i.e., on the errors associated with the solution of these equations, viz., programming of the code, discretization of partial differential equations, solution of the discretized equations, and computer accuracy. Furthermore, verification tasks can be further divided into tasks of verification of numerical codes and tasks of verification of numerical solutions. In this context, the studies carried out in this work are focused on the verification of numerical solutions, that is, in the development and assessment of a reliable methodology for the quantification in a statistical sense of the numerical uncertainty of computational solutions obtained from well-verified codes.

Although several alternative methods have been investigated for the verification of CFD solutions, e.g., methods based on the least-squares extrapolation [3] or on the error transport equation [4], those based on systematic grid refinement studies and the Richardson extrapolation techniques have probably been the most reliable and widely used for such purposes. These methods provide an estimation of the exact solution of the equations being solved, $\phi_E$, by extrapolating from the solutions reported on a set of systematically refined grids, as described in Section 2.1. As a first approach, the discretization error $e_D$ of a given numerical solution $\phi$ could be estimated from the extrapolated value of the exact solution, $\phi_{\text{extr}}$, as $\phi - \phi_{\text{extr}}$. However, a value of $e_D$ evaluated directly in this way does not provide, in general, a good confidence interval for nontrivial and nonlinear problems. Such limitation on the estimation of $e_D$ can be acknowledged by applying a safety or correction factor, obtaining, typically, an error band rather than an estimation of $e_D$ itself. However, the nature of this safety or correction factor differs for different authors. The verification methodology discussed in this work is based on the approach

proposed by Roache [5] and applied by authors in different fields (e.g., [6]). The underlying idea is the estimation of an error band, the grid convergence index (GCI), by multiplying the absolute value of the estimate of $e_D$ by a safety factor. The value of this factor is based on cumulative experience, depends exclusively on the number of solutions available for extrapolation, and aims at a 95% confidence interval. An alternative approach has been proposed by Stern et al. [7], where the error interval is calculated via the use of a correction factor that accounts for differences between the observed order of convergence and either the theoretical order of accuracy, or the order of convergence observed on solutions for simplified geometry and conditions.

Despite the effort given to the development of these verification methodologies, compelled by the urgent need in the CFD community to assess the credibility of the solutions obtained, and the relative success achieved in certain applications, at present, verification of CFD solutions is still far from being a completely mature and consolidated technique. For methods based on Richardson extrapolation techniques, difficulties arise in meeting the hypothesis assumed. Considering an expansion series of $\phi$, such as that of Eq. (2), the generalized Richardson extrapolation (GRE) estimates $\phi_E$ assuming that the leading-order term of this series dominates the discretization error. The order $p$ of this term must then be either assumed, or estimated from the observed convergence of $\phi$. Consequently, if a wrong value of $p$ is assumed, or if more than one term of the error series dominate the error, the GRE will fail to provide accurate estimations of $\phi_E$. Unfortunately, such asymptotic behavior of the solution convergence is seldom reached in practical cases. Contrarily, additional error terms of different order have been observed to also have, in general, a noticeable weight in the discretization error, resulting in mixed-order convergence of $\phi$. Furthermore, under such circumstances, if the leading error terms have different sign, nonmonotonic or oscillatory convergence may occur. As a result, as discussed in Section 2.1.1, unrealistic estimations of $p$ can be obtained, which would lead to highly inaccurate estimates of $\phi_E$. Moreover, in those cases where the values of $\phi$ obtained on the grid levels used for extrapolation do not show monotonic convergence, $p$, and therefore $\phi_E$, cannot be estimated. Nonmonotonic convergence may arise specially in those cases where mixed-order methods are used in the discretization of the governing partial differential equations. The use of these methods is indeed a common practice in CFD. Illustrative examples can be found in the discretization of: (1) different terms of a given equation, e.g., upwind (UDS) for the convective terms and central difference schemes (CDS) for the diffusive terms; (2) different coordinate directions, e.g., different order discretization in time and space coordinates; (3) different equations, e.g., first-order discretization of turbulence transport equations and second-order of the momentum equations; or (4) when hybrid methods, such as the SMART scheme [8], or flux limiters, are used.

These limitations of the GRE for verification purposes have been addressed in previous works by various authors. As a result, different strategies to tackle this issue have been proposed. Celik and Karatekin [9] introduced modifications in the way the observed order of accuracy, $p$, is calculated, to deal with oscillatory solution convergence and to prevent negative values of $p$. Additionally, the values of $p$ used for extrapolation were limited to a certain range given by the theoretical order of

accuracy of the discretization scheme. Cadafalch et al. [10] used the GRE in combination with an averaged value of $p$, calculated at all the nodes of the domain which converge monotonically. This value was expected to be contained within the limits of the theoretical $p$ for the method to be reliable. Additionally, low values of the standard deviation of $p$ are also required. As an alternatively to the use of the GRE, the multiexponent, or mixed-order Richardson extrapolation (MORE) [11, 12] can be used for the estimation of $e_D$, as in the works of Roy [13] and Roy et al. [14] This technique considers additional error terms, allowing the estimation of $\phi_E$ in nodes reporting monotonic or oscillatory convergence. A different strategy was developed by Eça and Hoekstra [15]. These authors estimated the observed $p$ with the least-squares root technique, and limited the use of the GRE to a given range of the local observed $p$. Outside this range, different extrapolation techniques, encompassing the multiexponent extrapolation, were used.

The application of any verification method to multidimensional solutions can be carried out based on two different approaches. On the one hand, the simultaneous coordinate refinement method (SCR) conducts grid refinement studies by simultaneously refining the grid in all coordinate directions using, in general, the same refinement ratio. On the other hand, the independent coordinate refinement method (ICR) [5], performs independent grid refinement studies for each independent coordinate direction. As a result, convergence information and values of the GCI are obtained for each independent coordinate. The overall value of the GCI can then be calculated from the values obtained for each coordinate. As is demonstrated later in this article, the information provided by the ICR method has been found to be useful to obtain accurate values of the GCI in certain cases where the SCR method failed. Such cases are characterized by the mixed-order discretization in different coordinate directions, causing the solution to converge nonasymptotically.

In this section, alternative verification strategies based on the Richardson extrapolation family have been introduced. Such strategies are based on the use of one, or a combination, of the following approaches to predict the uncertainty associated with a given solution: (1) use of the GRE in combination with the local bounded values of the observed $p$; (2) use of the GRE based on the global observed $p$; (3) use of the MORE. Furthermore, both the SCR and ICR approaches to deal with multidimensional solutions have been presented. It has also been mentioned that the verification of numerical solutions is still far from being a completely mature discipline. In this context, and by analyzing the results obtained in a number of representative test cases, this work seeks answers to some of the questions that still remain open: (1) How do the different methods compare in terms of accuracy and conservativeness? (2) Does $\mathrm{Fs} = 1.25$ provide the required conservativeness for all the methods tackled in this work? (3) Which limits should be applied to the local observed $p$ when used with the GRE? (4) Which error terms should be considered in MORE-based methods? (5) Is the global $p$ an adequate parameter based on which the limits of the observed local $p$ and the error terms considered in MORE can be chosen? (6) What are the benefits of the ICR strategy over the SCR? The remainder of this work is structured as follows. First, in Section 2 the fundamentals of solution verification methods based on Richardson extrapolation techniques and the GCI are addressed. A detailed verification procedure based on the different uncertainty estimation methods is described in Section 3. This is followed by descriptions of test

cases and discussion of results in Sections 4 and 5, respectively. Final conclusions and remarks are presented in Section 6.

## 2. FUNDAMENTALS

This section tackles fundamental topics in the verification of numerical solutions based on systematic grid refinement studies. The issues discussed encompass extrapolation techniques, error estimation and banding, alternative verification strategies, and specific aspects of the verification of multidimensional and transient solutions. The methodology presented is applied on a point-by-point basis. However, it can also be applied to global parameters, e.g., drag and lift coefficients, Nusselt numbers, etc.



### 2.1. Extrapolation Techniques

Let $\phi(\mathbf{x}, t)$ be a numerical solution, obtained at a given point $\mathbf{x}$ and instant $t$, which is free of both convergence and round-off errors, and which has been obtained from a verified code. Consider now the following power series representation of the local solution $\phi(\mathbf{x}, t)$:

$$\phi(\mathbf{x}, t) = \phi_E(\mathbf{x}, t) + C_1(\mathbf{x}, t)h + C_2(\mathbf{x}, t)h^2 + C_3(\mathbf{x}, t)h^3 + \cdots \tag{1}$$

where $h$ is a discretization parameter representative of the spatial and temporal grid, the coefficients $C_1(\mathbf{x}, t)$, $C_2(\mathbf{x}, t)$, $C_3(\mathbf{x}, t)$, ... are given by continuous functions dependent on the discretization scheme but not on the discretization grid, and where $\phi(\mathbf{x}, t)$ tends to the exact solution $\phi_E(\mathbf{x}, t)$ as the grid is refined. Assuming that the solution $\phi(\mathbf{x}, t)$ has been obtained from a $p$th-order-accurate numerical scheme, the coefficients $C_1(\mathbf{x}, t), \ldots, C_{p-1}(\mathbf{x}, t)$ will be zero, and Eq. (1) can then be rewritten as

$$\phi(\mathbf{x}, t) = \phi_E(\mathbf{x}, t) + C_p(\mathbf{x}, t)h^p + C_{p+1}(\mathbf{x}, t)h^{p+1} + C_{p+2}(\mathbf{x}, t)h^{p+2} + \cdots \tag{2}$$

The basic idea on which Richardson extrapolation techniques are based is that, as the grid is refined and $h$ takes smaller values, higher-order terms in Eq. (2) become smaller and eventually negligible. The generalized Richardson extrapolation (GRE) constitutes a first approach on which exclusively the $p$th-order term is considered for extrapolation. Alternatively, the multiexponent or mixed-order Richardson extrapolation technique (MORE) constitutes a higher-order approach, as higher-order terms in Eq. (2) are taken into account.

**2.1.1. Generalized Richardson extrapolation (GRE).** Assuming that the $p$th-order term in the series (2) prevails over the higher-order terms, $\phi(\mathbf{x}, t)$ can be expressed as

$$\phi(\mathbf{x}, t) \cong \phi_E(\mathbf{x}, t) + C_p(\mathbf{x}, t)h^p \tag{3}$$

As a first approach, $p$ can be assumed from the theoretical order of accuracy of the discretization scheme. If so, $\phi_E(\mathbf{x}, t)$ can be calculated from a set of two solutions,

$\phi_1(\mathbf{x}, t)$ and $\phi_2(\mathbf{x}, t)$, obtained on the grid refinement levels, $h_1$ and $h_2$. However, it is preferred to estimate the value of $p$ rather than assuming it. This can be done by using a third numerical solution, $\phi_3(\mathbf{x}, t)$, obtained in an additional grid level $h_3$. Proceeding this way, if a constant grid refinement ratio $r = h_2/h_1 = h_3/h_2$ is assumed, the values of $p(\mathbf{x}, t)$ and $\phi_E(\mathbf{x}, t)$ can be obtained from expressions

$$p(\mathbf{x}, t) = \frac{\ln[\varepsilon_{32}(\mathbf{x}, t)/\varepsilon_{21}(\mathbf{x}, t)]}{\ln(r)} \tag{4}$$

$$\phi_E(\mathbf{x}, t) \cong \phi_{\text{extr}}(\mathbf{x}, t) = \phi_1(\mathbf{x}, t) + \frac{\varepsilon_{21}(\mathbf{x}, t)}{1 - r^{p(\mathbf{x},t)}} \tag{5}$$

where

$$\varepsilon_{21}(\mathbf{x}, t) = \phi_2(\mathbf{x}, t) - \phi_1(\mathbf{x}, t) \tag{6}$$

$$\varepsilon_{32}(\mathbf{x}, t) = \phi_3(\mathbf{x}, t) - \phi_2(\mathbf{x}, t) \tag{7}$$

According to Eq. (5), the exact solution $\phi_E(\mathbf{x}, t)$ is estimated from the extrapolated value, $\phi_{\text{extr}}(\mathbf{x}, t)$. The local order of accuracy $p(\mathbf{x}, t)$ calculated from Eq. (4) is referred to as the *observed order of accuracy*. It must be noted that if the solution is converging nonmonotically, the ratio $\varepsilon_{32}(\mathbf{x}, t)/\varepsilon_{21}(\mathbf{x}, t)$ can take negative values, in which case Eq. (4) would then be undefined. Additionally, nonmonotonic solution convergence can also lead to Eq. (4) to provide highly unrealistic values of $\phi_E(\mathbf{x}, t)$. Consequently, it is advisable to limit somehow the values of $p(\mathbf{x}, t)$ used in Eq. (5) to values within a certain realistic range. How this range can be selected, and its effects on the accuracy of the verification method, is addressed in the following sections of this work. Furthermore, if the ratio $\varepsilon_{32}(\mathbf{x}, t)/\varepsilon_{21}(\mathbf{x}, t)$ is negative, Eq. (4) will provide nonreal values of $p(\mathbf{x}, t)$.

Finally, if $\phi_E(\mathbf{x}, t)$ is available by whatever means, as in the manufactured solution created for test case A of this work (see Section 4.1), the value of $p(\mathbf{x}, t)$ can be easily obtained from Eq. (3) on two different grid levels,

$$p_r(\mathbf{x}, t) = \frac{\ln[e_2(\mathbf{x}, t)/e_1(\mathbf{x}, t)]}{\ln(r)} \tag{8}$$

where $e_1(\mathbf{x}, t)$ and $e_2(\mathbf{x}, t)$ are the values of the exact error in grid levels 1 and 2, respectively,

$$e_1(\mathbf{x}, t) = \phi_1(\mathbf{x}, t) - \phi_E(\mathbf{x}, t) \tag{9}$$

$$e_2(\mathbf{x}, t) = \phi_2(\mathbf{x}, t) - \phi_E(\mathbf{x}, t) \tag{10}$$

It must be noted that $p_r(\mathbf{x}, t)$ is the value of $p(\mathbf{x}, t)$ needed for Eq. (5) to provide $\phi_E(\mathbf{x}, t)$, and will be the real order of convergence of the solution only if the error is truly dominated by one term, as assumed in Eq. (3). Therefore, the higher the deviation of $p(\mathbf{x}, t)$ from $p_r(\mathbf{x}, t)$, the less accurate will be the value of $\phi_{\text{extr}}(\mathbf{x}, t)$ obtained from Eq. (5).

**2.1.2. Mixed-order Richardson extrapolation (MORE).** Extrapolations of higher order than the GRE can be obtained by considering additional error terms in Eq. (2) [11, 12]. Let us assume now that the discretization error in Eq. (1) is dominated by both the first- and second-order error terms:

$$\phi(\mathbf{x}, t) \cong \phi_E(\mathbf{x}, t) + C_1(\mathbf{x}, t)h + C_2(\mathbf{x}, t)h^2 \tag{11}$$

Given a set of three numerical solutions obtained on the grid triplet $h_1 = h_2/r = h_3/r^2$, $\phi_E(\mathbf{x}, t)$ can be estimated as

$$\phi_E(\mathbf{x}, t) \cong \phi_{\text{extr}}(\mathbf{x}, t) = \phi_1(\mathbf{x}, t) + \frac{\varepsilon_{32}(\mathbf{x}, t) - (r^2 + r - 1)\varepsilon_{21}(\mathbf{x}, t)}{(r+1)(r-1)^2} \tag{12}$$

In the particular case of $r = 2$, Eq. (12) reduces to

$$\phi_E(\mathbf{x}, t) \cong \phi_{\text{extr}}(\mathbf{x}) = \phi_1(\mathbf{x}, t) + \frac{1}{3}(\varepsilon_{32} - 5\varepsilon_{21}) \tag{13}$$

If both second- and third-order error terms are considered to dominate the discretization error, the following expression can be similarly obtained for the estimation $\phi_E(\mathbf{x}, t)$ in case where $r = 2$:

$$\phi_E(\mathbf{x}, t) \cong \phi_{\text{extr}}(\mathbf{x}) = \phi_1(\mathbf{x}, t) + \frac{1}{21}(\varepsilon_{32} - 11\varepsilon_{21}) \tag{14}$$

The multiexponent extrapolation technique exposed here is based on considering for extrapolation exclusively two error terms, the order of which must be assumed from the discretization scheme if only three grid refinement levels are considered for extrapolation. If solutions obtained on additional grid levels are available, alternative and, in general, more accurate techniques can be applied. Such alternatives are based on either considering additional error terms for extrapolation, or the estimation of the order of these terms rather than assuming them. However, with the aim of comparing methods with similar computational costs, only methods based on the use of three grid refinement levels have been considered in this work.

## 2.2. The Grid Convergence Index (GCI)

The extrapolation techniques presented in Sections 2.1.1 and 2.1.2 provide an estimation of the exact solution, from which the discretization error can easily be estimated as

$$e_D(\mathbf{x}, t) \approx \phi(\mathbf{x}, t) - \phi_{\text{extr}}(\mathbf{x}, t) \tag{15}$$

However, for verification purposes, Eq. (15) does not, in general, provide estimations of $e_D(\mathbf{x}, t)$ that are sufficiently accurate for nontrivial and nonlinear problems. The GRE and MORE techniques require that solutions converge asymptotically toward $\phi_E$ under the hypothesis assumed. Contrarily, it is found in practice that

reaching the asymptotic range can require the use of excessively dense grids, usually too expensive from a computational point of view. However, despite the limited accuracy of the exact solution estimations and, therefore, of the associated discretization error, this value is still of interest to provide information on the credibility of numerical solutions. Toward this objective, Roache [5], based on cumulative experience, multiplied $|e_D(\mathbf{x}, t)|$ by a safety factor $F_s$ to obtain an error band within which the exact error was expected to be included with a confidence interval of 95%. Roache referred to the resulting error band as the grid convergence index, which is defined as:

$$\mathrm{GCI}(\mathbf{x}, t) = F_s|e_D(\mathbf{x}, t)| = F_s|\phi(\mathbf{x}, t) - \phi_{\mathrm{extr}}(\mathbf{x}, t)| \tag{16}$$

For studies based on the use of only two grid refinement levels, a conservative value of $F_s = 3$ is recommended. For higher-quality grid convergence studies reporting solutions on a minimum of three grids, a value of $F_s = 1.25$ is considered to be sufficiently conservative. However, it can be questioned at this point whether this is an adequate value for any verification procedure based on three grid levels, regardless of the extrapolation strategy adopted or the discretization schemes used. It is shown in the results section of this work that the use of $F_s = 1.25$ can lead to either underpredictions of the error band, or to overly conservative predictions, unless adequate estimations are made of the values of $p$, in the GRE, or in the choice of the error terms, in the MORE.

### 2.3. Verification Strategies Based on the Richardson Extrapolation Techniques

It has already been introduced in Section 1 that nonmonotonic or oscillatory convergence can arise in those cases where mixed-order solution convergence occurs. In such cases, Eq. (4) can provide highly unrealistic values of $p(\mathbf{x}, t)$, which would lead to inaccurate estimations of the GCI. Furthermore, if $\varepsilon_{32}/\varepsilon_{21}$ is negative, Eq. (4) is undefined, and $p(\mathbf{x}, t)$ cannot be estimated. In order to tackle these issues, various procedures can be adopted. These procedures can be grouped into three different general strategies. The first strategy uses the GRE and the local observed order of convergence, which is limited to a certain range of realistic values. However, as is proved in Section 5, this strategy still leaves open issues such as what should be the bounds of the range, or what strategy should be adopted when values of $p(\mathbf{x}, t)$ outside this range are obtained. Illustrative examples on how these issues have been addressed by different authors can be found, for instance, in the work of Celik and Karatekin [9] and of Eça and Hoekstra [15]. In both works, different procedures were adopted for cases of mixed first- and second-order discretizations. Celik and Karatekin studied the turbulent flow past a backward-facing step using nonuniform grid distribution. The solutions were obtained from a code using a hybrid of the first-order upwind scheme (UDS) and the second-order central differencing scheme (CDS). In this work, the authors introduced modifications in the way $p(\mathbf{x}, t)$ was calculated, and limited the minimum and maximum values to the theoretical limits, i.e., $1 < p(\mathbf{x}, t) < 2$. In order to ensure positive values of $p(\mathbf{x}, t)$, and therefore error convergence toward 0 as the grid is refined, the absolute value was applied on the

right-hand side of Eq. (4). Also, for nonmonotonic convergence where the error decreases with alternating sign, the sign of the error on the second grid level was changed. A different strategy was adopted by Eça and Hoekstra, who studied the 2-D, incompressible, turbulent flow on a flat channel. In this case, the continuity and the momentum equations were discretized second-order, while turbulent quantities transport equations were discretized first-order. The observed order of accuracy was estimated with the least-square root technique. Different extrapolation techniques, encompassing GRE and MORE, in combination with different values of $F_s$, were used depending on the values of the observed order of accuracy.

The second of the strategies mentioned above is based on the GRE in combination with an averaged value of $p$, calculated at all the domain nodes which report monotonic convergence. This idea was introduced by Cadafalch et al. [10], who considered it plausible to expect an overall order of accuracy $p$ bounded by the order of accuracy of the schemes used. Under such conditions, the numerical solution converges asymptotically, observing the assumptions of the Richardson extrapolation. Furthermore, the standard deviation of $p(\mathbf{x}, t)$, $\sigma_p$, was also calculated. This value was taken as a measure of the proximity to the asymptotic range, and therefore of the credibility of the estimates obtained. The authors reported a wide range of steady-state test cases, encompassing applications on both laminar and turbulent flows with different configurations, and in a premixed methane/air laminar flat flame. Both the UDS and the hybrid SMART schemes were used for discretization. Roache's $F_s = 1.25$ was applied in all cases. As a conclusion of this work, the authors stated that although the procedure proved to be reasonably reliable for all the studied cases, further research was still required to investigate the reliability of the procedure in other kind of flows. In this sense, the results reported in Section 5 reveal limitations of the method in the test cases analysed.

Problems associated with the nonasymptotic convergence of solutions can be partly overcome by the mixed-order Richardson extrapolation based on three grid levels discussed in Section 2.1.2. This technique, which constitutes the third of the strategies mentioned above, can deal with nonmonotonic solution convergence, providing estimates of $\phi_E(\mathbf{x}, t)$ in all cases. However, the estimates obtained will only be accurate if the error is truly dominated exclusively by two terms, and the order of these terms is correctly assumed. This is the critical point when MORE based on three grid levels is used. It is not always an easy exercise to decide which terms will dominate the error. Consider, for example, a numerical solution that has been obtained using a mixed-order discretization method. Let us also assume that a hybrid method, such as SMART, which is a bounded scheme that can behave first-, second-, or third-order, has been used in the discretization of the convective terms [16]. Finally, assume that discretization of the governing equations has been completed with a combination of methods of different order, e.g., first-order fully implicit in time, CDS for the diffusive term, etc. This can be indeed a common case, representative of common computations, where the dominating error terms are not known beforehand. Rather, the error will be dominated by different terms depending on the particular cases being studied and the size of the space and time grids being used. In a case like this, and lacking previous experience from similar cases, it can be difficult to decide which terms will dominate the error, or whether the convergence of the solutions can accurately be described with only two error terms.

A verification procedure encompassing the three verification strategies above discussed, viz., the GRE based on local bounded $p(\mathbf{x}, t)$, the GRE based of the overall $p$, and the three-grid-levels MORE, is presented in Section 3. The performance of these strategies is further analyzed in the results section.

### 2.4. Multidimensional Solutions

As introduced in Section 1, the verification of multidimensional CFD solutions can be addressed with both the simultaneous coordinate refinement (SCR) and the independent coordinate refinement (ICR) methods. Before getting into further detail about these methods, it must be noted that within the framework of this work, the time coordinate is considered in just the same way as any of the space coordinates. This way, the term "multidimensional" comprises both the time and space coordinates. On the one hand, SCR is the most common approach for the verification of steady multidimensional solutions. In this approach, the discretization grid is simultaneously refined in all coordinate directions using in general the same grid refinement ratio $r$. This method therefore provides information on the convergence of the overall error associated with the discretization of all coordinate directions (space and time).

On the other hand, in the ICR approach, grid refinement studies are conducted independently on each independent coordinate direction, while the grid on the rest of coordinates is kept constant. Consequently, as grid refinement studies are conducted independently, different techniques can be applied for the estimation of the error associated with the discretization on each direction, i.e., different values of $r$, different extrapolation techniques, or even alternative methods not based on grid refinement studies. Also, as more grid refinement studies are conducted, and therefore solutions from a larger number of meshes are used, additional information on the error convergence associated with the discretization of each independent coordinate is provided. As discussed in Section 5, this additional information has proved to be useful for the verification of certain solutions where the STD method fails to provide accurate estimators of the discretization error. As a drawback, the larger number of solutions required can increase the computational cost associated with this approach. This cost, however, can be reduced if the coarsest grid level is used on the independent coordinates that are not being refined. The ICR approach can become particularly adequate for solutions where mixed-order discretization in different coordinate directions leads to nonmonotonic error convergence. This can be the case, for instance, for transient solutions where schemes of different order are used on both the space and the time discretization, e.g., a first-order, fully implicit time discretization in combination with a second-order space discretization. Results for similar cases are discussed in Section 5.

Following Roache's reasoning based on the multidimensional theory [5], the overall value of the GCI in ICR studies can be evaluated from the estimates of the discretization error obtained in each direction. Roache suggests the following expression to calculate the overall GCI:

$$\mathrm{GCI}(\mathbf{x}, t) = \mathrm{GCI}_x(\mathbf{x}, t) + \mathrm{GCI}_y(\mathbf{x}, t) + \mathrm{GCI}_z(\mathbf{x}, t) + \mathrm{GCI}_t(\mathbf{x}, t) \tag{17}$$

where the subscript *x, y, z*, or *t* refers to the values obtained from the corresponding coordinate refinement study keeping constant the other coordinates.

Aspects related to the accuracy of Eq. (17) will be discussed in Section 5, where an alternative expression, based on the addition of discretization errors rather than the GCI, will be proposed and briefly investigated.

In transient cases, if the ICR approach is applied to study independently the error convergence associated with the space and the time discretizations, Eq. (17) can be rewritten as:

$$\mathrm{GCI}(\mathbf{x}, t) = \mathrm{GCI}_s(\mathbf{x}, t) + \mathrm{GCI}_t(\mathbf{x}, t) = F_s|e_{D,s}(\mathbf{x}, t)| + F_s|e_{D,t}(\mathbf{x}, t)| \tag{18}$$

where subscript *s* refers to values obtained from SCR studies conducted on the space coordinates while keeping the time grid constant.



## 3. VERIFICATION PROCEDURE

The procedure presented here has been developed as an extension of the postprocessing tool for the verification of steady-state solutions reported by Cadafalch et al. [10]. The tool is based on the GRE and the global observed value of *p*, and provides information on both the local and global estimates of the observed order of accuracy and the GCI. Initially, all solutions are interpolated onto a common postprocessing mesh. Nodes of this mesh are then classified into Richardson, oscillatory, and converged nodes, depending on the local observed convergence behavior. Local estimators of *p* are then calculated at all the Richardson nodes, and of the GCI at both Richardson and converged nodes. This tool, based on SCR studies, can be applied to the verification of transient solutions by simply considering the time coordinate in the same way as the rest of the space coordinates. The present procedure includes additional grid extrapolation techniques, namely, the GRE based on the local bounded *p*, the GRE based on the global *p*, and the MORE. Furthermore, the procedure has also been further extended to ICR studies.

The procedure described below is divided into two parts. Part I applies to both SCR and ICR studies. For the latter, the procedure must be carried out for each independent coordinate direction. Information on the convergence associated with the discretization of each of these directions is provided. Part II applies exclusively to ICR studies, and provides the overall values of both the local and the global GCI.

### Part I (For SCR and ICR Studies)

**Step 1. Interpolation at the post-processing mesh.** All three solutions are interpolated into the nodes of the grid where the estimators are calculated (the postprocessing mesh), typically the coarsest grid. Special care is taken to avoid the introduction of additional uncertainties due to the interpolation process by using third-order-accurate Lagrangian interpolation.

**Step 2. Classification of the calculation nodes.** All the calculation nodes of the postprocessing mesh are classified into Richardson, converged, or oscillatory nodes, according to the following definitions,

Richardson node: $\varepsilon^*_{32}(\mathbf{x}, t) \cdot \varepsilon^*_{21}(\mathbf{x}, t) > C_0$
Converged node: $|\varepsilon^*_{32}(\mathbf{x}, t) \cdot \varepsilon^*_{21}(\mathbf{x}, t)| \leq C_0$
Oscillatory node: $\varepsilon^*_{32}(\mathbf{x}, t) \cdot \varepsilon^*_{21}(\mathbf{x}, t) < -C_0$

where the superscript $^*$ indicates that the solutions have been normalized by means of the maximum absolute value of $\phi(\mathbf{x}, t)$, and $C_0$ is a positive coefficient approaching 0. As in the work by Cadafalch et al., $C_0 = 10^{-30}$ is used in this work, where computations have also been performed using double-precision real numbers. It must be noted that the definition of Richardson nodes in this classification coincides with that of nodes showing monotonic error convergence, rather than those in which the asymptotic convergence requirement of the GRE is fulfilled.

**Step 3. Calculation of the local observed order of accuracy, *p*(x, *t*).** Local values of the observed order of accuracy $p(\mathbf{x}, t)$ are calculated on Richardson nodes from Eq (4).

**Step 4. Calculation of the global observed order of accuracy, *p*.** The global observed order of accuracy is evaluated by arithmetic averaging of all values of the observed $p(\mathbf{x}, t)$ at the Richardson nodes. The standard deviation of the local values from the mean values, $\sigma_p$, is also calculated.

**Step 5. Calculation of the local GCI.** The values of GCI( $\mathbf{x}$, $t$) are calculated for the solution obtained on the fine grid from Eq. (16) using a safety factor $F_s = 1.25$. Depending on the extrapolation technique adopted for the estimation of $\phi_E(\mathbf{x}, t)$, the following methods have been considered.

*STD (standard) method*. The local GCI is calculated at all the Richardson and converged nodes. At the Richardson nodes, GCI($\mathbf{x}$, $t$) is evaluated using the extrapolated value obtained from Eq. (5), assuming $p(\mathbf{x}, t)$ to be equal to the global observed order of accuracy, $p$, calculated at Step 4. At the converged nodes, GCI($\mathbf{x}$, $t$) is assumed to be 0.

*LP methods*. This is similar to the STD method, except for the estimation of $p(\mathbf{x}, t)$. This value is now calculated from Eq. (4) if it is contained within a certain range, $p_L \leq p(\mathbf{x}, t) \leq p_U$. Otherwise, the values of the upper and lower bounds of this range, $p_U$ and $p_L$, are used, depending on whether $p(\mathbf{x}, t)$ sits above or below this range, respectively. Depending on the values of $p_L$ and $p_U$, three different variants are considered, LP12, LP13, and LP23, which are characterized by bounds $1.0 \leq p(\mathbf{x}, t) \leq 2.0$, $1.0 \leq p(\mathbf{x}, t) \leq 3.0$, and $2.0 \leq p(\mathbf{x}, t) \leq 3.0$, respectively.

*MO methods*. The local GCI is calculated from the mixed-order Richardson extrapolation (MORE) at all the postprocessing mesh nodes. Two different methods have been considered. Method MO12 is based on the mixed first- and second-order extrapolation, and estimates $\phi_E(\mathbf{x}, t)$ from Eq. (13). Method

MO23 is based on the mixed second- and third-order extrapolation, and estimates $\phi_E(\mathbf{x}, t)$ from Eq. (14).

**Step 6. Calculation of the global GCI.** The global value of the GCI is estimated by volume-weighted averaging of the local values of the GCI. The global GCI is calculated from local values at the Richardson and the converged nodes for the STD and the LP methods. For the MO methods, the global GCI is calculated from local values at all the postprocessing mesh nodes. The standard deviation of the GCI can also be calculated.



### Part II (Only for ICR Studies)

**Step 1. Calculation of the local values of the overall GCI.** These values are calculated from Eq. (17) at all nodes of the postprocessing mesh where the local GCI values could be estimated according to Step 5 of Part I for all the independent coordinate directions.

**Step 2. Calculation of the global value of the overall GCI.** This value is calculated as

$$\mathrm{GCI} = \mathrm{GCI}_x + \mathrm{GCI}_y + \mathrm{GCI}_z + \mathrm{GCI}_t \tag{19}$$

where the terms on the right-hand side of the equation correspond to the global GCI values (see Step 6 of Part I) obtained in the respective coordinate directions ($x, y, z, t$). The idea behind this expression is just the same as in Eq. 17 but applied to the global values of the GCI rather than to the local ones.

It must be noted that, alternatively, the global value of the overall GCI (Part II, Step 2) could also have been calculated based on volume averaging of the local values of the overall GCI. This option, however, has a practical disadvantage. If GRE is used for extrapolation in different coordinate directions, the number of nodes where the local GCI can be calculated for each one of the independent coordinates can be, in practice, quite reduced. As a result, in general, less reliable global values of the overall GCI can be obtained.

## 4. TEST CASES

The following test cases have been selected to assess the accuracy and the conservativeness of the verification methods discussed in this work. The first case is based on the method of manufactured solutions (MMS) [17]. This method forces the governing equations to provide a certain manufactured analytical solution, regardless of its physical realism, by including the required additional source terms. The accuracy and the conservativeness of the estimators obtained from the different verification methods being studied can therefore be assessed by simply comparison with the values of the exact error. In the second and third cases, the fluid flows for two different piston–cylinder configurations are studied.

The solutions of all three test cases have been computed using the finite-volume method based on staggered arrangement of variables. The segregated SIMPLEC [18]

**Table 1.** Space and time discretization grids used in the test cases

| Cases A and C | | | | Case B | | | |
|---|---|---|---|---|---|---|---|
| Space grid | | Time grid | | Space grid | | Time grid | |
| Level | Size | Level | Size | Level | Size | Level | Size |
| m1 | $6 \times 6$ | t1 | 60 | m1 | $10 \times 20$ | t1 | 204 |
| m2 | $12 \times 12$ | t2 | 120 | m2 | $19 \times 41$ | t2 | 408 |
| m3 | $24 \times 24$ | t3 | 240 | m3 | $38 \times 82$ | t3 | 816 |
| m4 | $48 \times 48$ | t4 | 480 | m4 | $76 \times 164$ | t4 | 1,632 |
| m5 | $96 \times 96$ | t5 | 960 | m5 | $152 \times 328$ | t5 | 3,264 |
| m6 | $192 \times 192$ | t6 | 1920 | m6 | $304 \times 656$ | t6 | 6,528 |



algorithm has been used to deal with the pressure–velocity coupling. The calculation domains have been discretized using Cartesian moving grids. The hybrid SMART scheme is used in the discretization of the convective term, while CDS is used for the diffusive term, and formally second-order methods are used for the remaining terms. Both first- (1OT) and second-order (2OT) fully implicit discretizations have been used for time discretization. Satisfaction of the discrete space conservation law has been enforced. The sets of grids used in the discretization of each case are tabulated in Table 1. To avoid confussion, it must be noted that, contrary to criteria followed in Section 2.1, the grid indices in Table 1 increase as the grid is refined. A well-verified code, DPC [10], has been used to perform the computation of the solutions of all three test cases. Let test case A serve as an example of the thorough verification testing that has been conducted on this code.

### 4.1. Case A: Manufactured Solution

The MMS is applied to the axisymmetric, incompressible continuity and momentum equations. The proposed manufactured solution is

$$v_r = V_0 \sin(r) \sin(z) \sin(t) \tag{20}$$

$$v_z = V_0 \frac{\cos(z) \sin(t)[\sin(r) + r \cos(r)]}{r} \tag{21}$$

$$p = r^3 + z^3 \tag{22}$$

where $r$ and $z$ are the radial and axial components of the position vector, respectively; $t$ is the time; $v_r$ and $v_z$ are the radial and axial components of the velocity vector; $p$ is pressure; and $V_0$ is a reference velocity equal to 1. The equations are solved in the domain $D = \{(r,\ z) \,|\, r \in [\pi,\ 2\pi],\ z \in [0,\ 2\pi]\}$ from the initial instant $t_0 = 0$ to the final instant $t_f = 6$. The calculation domain is discretized using moving grids with fixed boundaries. The motion of the mesh is achieved by varying the concentration of the nodes toward the boundaries in each direction. The grid concentration is controlled by the hyperbolic tangent concentration function reported by

Pérez-Segarra et al. [19], using a grid concentration factor $\gamma = \sin(t)$. A uniform grid has been used for time discretization. A Reynolds number ($\mathrm{Re} = \rho V_0 \pi/\mu$) of $100\pi$ has been used. Dirichlet boundary conditions are determined from the manufactured solution. As an illustrative example of the manufactured solution studied, a plot of the stream traces at the instant $t/t_f = 0.75$ is given in Figure 1.

### 4.2. Case B: Incompressible Flow on a Piston–Cylinder Assembly

The incompressible, laminar, axisymmetric flow on the piston–cylinder assembly proposed by Durst et al. [20, 21] is analyzed. Figure 2 shows the geometry of the configuration under study. Flow starts from rest at $t = 0$, and the piston suddenly accelerates to its final velocity $V_p$. The characteristic dimensions of the domain sketched in Figure 2 are $l_i = 100\,\mathrm{mm}$, $d_i = 19\,\mathrm{mm}$, and $d_p = 45\,\mathrm{mm}$. The initial piston clearance is 40 mm at $t = 0$, and moves at $V_P = 11.9\,\mathrm{mm/s}$ during 2.04 s. The Reynolds number, defined as $\mathrm{Re} = \rho V_P d_i/\mu$, is 98. For the inlet boundary condition, the axial velocity has been assumed to be uniform, and the radial velocity to be zero. Nonslip boundary condition has been considered in the walls of the channel, the cylinder, and the piston head. The domain has been divided into the three different blocks shown in Figure 2 and a uniform grid has been used for the discretization of each block. Uniform time steps have been employed in time coordinate discretization.

### 4.3. Case C: Gas Spring

The two-dimensional, compressible flow in a closed piston–cylinder configuration is studied. Figure 3 sketches the geometry of the calculation domain, where

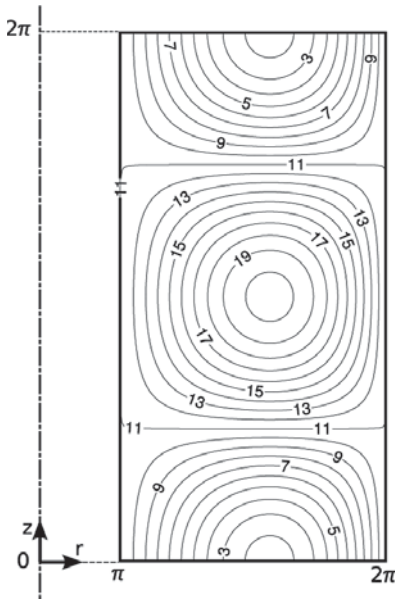


**Figure 1.** Case A. Manufactured solution. Stream traces at time instant $t/t_f = 0.75$.

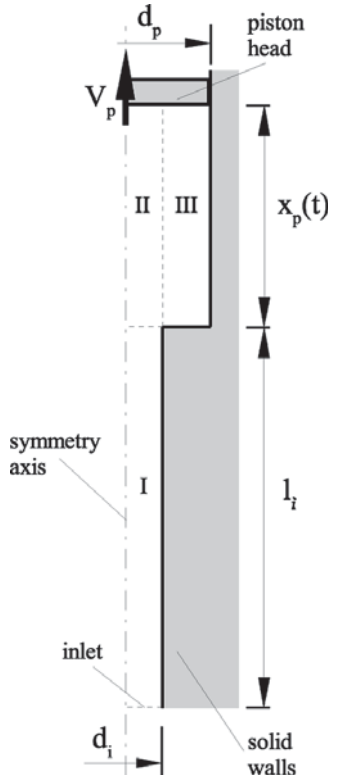


**Figure 2.** Case B. Incompressible flow on a piston–cylinder assembly.

the piston diameter and stroke are $d_p = 50.80\,\text{mm}$ and $L = 76.2\,\text{mm}$, respectively. The piston moves at $10\,\text{rev/min}$, following a sinusoidal law, with a compression ratio $r_P = 2$. One cycle of the movement of the piston is studied. Perfect gas

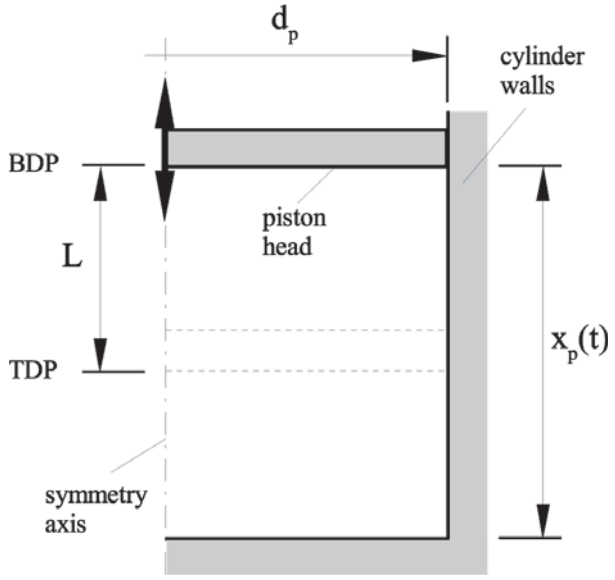


**Figure 3.** Case C. Gas spring.

assumption is made, with $\widetilde{R} = 2{,}077.0\,\mathrm{J/kg\,K}$ and $c_p = 5{,}192.50\,\mathrm{J/kg\,K}$. Transport thermodynamic properties are $\mu = 1.99 \times 10^{-5}\,\mathrm{kg/ms}$ and $\lambda = 0.152\,\mathrm{W/m\,K}$. Flow starts from rest conditions at 294 K and 101,325 Pa. Pressure, dissipation energy, and conduction heat terms have been evaluated in the thermal energy equation. A constant temperature of 294 K has been set at all walls of the domain, where nonslip boundary condition has been applied. Uniform time and space grids have been used.



## 5. RESULTS

This section tackles the assessment of the different verification methods considered in the procedure described in Section 3. All the methods investigated are summarized in Table 2, together with the nomenclature used in this section to refer to each method. In order to minimize the effects of the solution interpolation in Step 1 of the verification procedure, the coarsest grid of each triplet has been used as postprocessing mesh. The values of the percentage of Richardson nodes ($R_n$), the global observed $p$, and the standard deviation ($\sigma_p$) of the local observed $p(\mathbf{x}, t)$ have been tabulated for each grid triplet studied. Normalized values of the discretization error and the grid convergence index, $e_D^*$ and GCI$^*$, are provided as percentage of the reference values described in each test case. In ICR studies, the STD method has been used on both the space (HREF) and time (TREF) grid refinement studies. In these studies, the finest grid level of each grid triplet is used in the independent coordinate; e.g., on the sixth grid level (m6t6), the m6t4, m6t5, m6t6 triplet is used in TREF studies, and the m4t6, m5t6, m6t6 triplet in HREF studies. Finally, in the tables of results provided, the grid index refers to the mesh levels of the coordinate being refined. That is, grid indices 4/5/6, in SCR studies, refer to grids levels m4t4, m5t5, and m6t6, while, in ICR studies, these refer to m4t6, m5t6, m6t6 for HREF studies, and to m6t4, m6t5, m6t6 for TREF studies.

**Table 2.** Acronyms corresponding to the different verification methods

| Description | Acronym |
|---|---|
| Simultaneous space-and-time-coordinates refinement studies (SCR) | |
| GRE based on the global $p$ (*standard method*) | STD |
| GRE based on the local $p$ (*LP methods*) | |
| $1 \le p \le 2$ | PL12 |
| $1 \le p \le 3$ | PL13 |
| $2 \le p \le 3$ | PL23 |
| Mixed-order Richardson extrapolation (*MORE method*) | |
| First- and second-order | MO12 |
| Second- and third-order | MO23 |
| Independent coordinate refinement studies (ICR) | |
| HREF and TREF studies based on STD method | ICR-STD |

HREF and TREF refer to grid refinement in space and time coordinates, respectively.

### 5.1. Case A

Information on the global postprocessing estimators is given in Table 3 and in Figures 4–6, for both 1OT and 2OT discretization methods. The reported values of the GCI* and $e_D^*$ have been normalized using the velocity $V_0$ as reference value. Results show that high values of $R_n$ have been obtained in all the tested cases, where values equal to or higher than 90% are reported on the finest grid level. These values are particularly high for TREF studies, where $R_n$ reaches 100% of the calculation nodes. Under these conditions the global estimators $p$, $\sigma_p$, and the GCI* are considered to be representative of the global convergence of the solutions under analysis.

The results corresponding to the 1OT scheme clearly depict the conditions under which oscillatory convergence caused by mixed-order discretization on different coordinate directions can arise. On the one hand, different-order error convergence is observed from HREF and TREF studies, while HREF suggests a second-order trend, specially for $v_z$, TREF reports $p = 1.0$ and fairly low values of $\sigma_p$ for both components of the velocity. On the other hand, although not provided, the GCI values provided by HREF and TREF studies suggest that the overall error is dominated by both the space and time discretizations. Under such conditions of mixed-order convergence, SCR studies reveal a high dependence of $p$ on the grid refinement level, showing neither a clear first- nor second-order trend. Additionally, the differences between the values of $p$ and $p_r$ reported for 1OT in Table 3 advance the possibility of methods based on GRE being poorly accurate, therefore increasing the risk of underestimating the GCI.

Under such circumstances, despite the high number of Richardson nodes and that values of $p$ within the expected limits have been obtained, the STD method fails

**Table 3.** Case A: Manufactured solution, Richardson nodes, global $p$, and $\sigma_p$

| | | 1OT | | | | | | 2OT | | | | | |
|---|---|---|---|---|---|---|---|---|---|---|---|---|---|
| | | Radial velocity | | | Axial velocity | | | Radial velocity | | | Axial velocity | | |
| | Grid triplet | $R_n$ (%) | $p/p_r$ | $\sigma_p$ | $R_n$ (%) | $p/p_r$ | $\sigma_p$ | $R_n$ (%) | $p/p_r$ | $\sigma_p$ | $R_n$ (%) | $p/p_r$ | $\sigma_p$ |
| SCR | 1/2/3 | 81 | 1.7/1.6 | 1.3 | 84 | 1.3/1.5 | 1.5 | 79 | 1.7/1.8 | 1.5 | 83 | 1.4 /2.0 | 1.5 |
| | 2/3/4 | 83 | 1.7/1.5 | 1.6 | 90 | 1.8/1.3 | 1.2 | 82 | 1.9/2.2 | 1.7 | 89 | 2.0/2.0 | 1.2 |
| | 3/4/5 | 85 | 1.9/1.2 | 1.4 | 91 | 1.6/1.1 | 1.1 | 87 | 2.3/2.2 | 1.4 | 93 | 2.0/2.0 | 1.0 |
| | 4/5/6 | 90 | 1.4/1.1 | 1.2 | 93 | 1.4/1.1 | 1.0 | 93 | 2.2/2.1 | 1.0 | 96 | 2.0/2.0 | 0.7 |
| HREF | 1/2/3 | 79 | 1.8/— | 1.5 | 83 | 1.5/— | 1.4 | 78 | 1.8/— | 1.6 | 83 | 1.4/— | 1.4 |
| | 2/3/4 | 82 | 2.0/— | 1.7 | 88 | 2.0/— | 1.2 | 82 | 1.9/— | 1.7 | 88 | 2.0/— | 1.2 |
| | 3/4/5 | 87 | 2.3/— | 1.4 | 92 | 2.0/— | 1.0 | 87 | 2.3/— | 1.4 | 92 | 2.0/— | 1.0 |
| | 4/5/6 | 93 | 2.2/— | 1.0 | 96 | 2.0/— | 0.7 | 93 | 2.2/— | 1.0 | 96 | 2.0/— | 0.7 |
| TREF | 1/2/3 | 98 | 1.0/— | 0.5 | 96 | 1.0/— | 0.5 | 97 | 2.0/— | 0.7 | 96 | 2.0/— | 0.7 |
| | 2/3/4 | 99 | 1.0/— | 0.4 | 99 | 1.0/— | 0.4 | 98 | 2.0/— | 0.5 | 98 | 2.0/— | 0.5 |
| | 3/4/5 | 99 | 1.0/— | 0.3 | 99 | 1.0/— | 0.3 | 98 | 2.0/— | 0.3 | 99 | 2.0/— | 0.3 |
| | 4/5/6 | 100 | 1.0/— | 0.2 | 100 | 1.0/— | 0.2 | 100 | 2.0/— | 0.2 | 100 | 2.0/— | 0.2 |

For SCR studies, global values of $p_r$ are also provided. 1OT and 2OT refer to first- and second-order time discretization respectively. For grid triplets nomenclature, refer to introduction to Section 4. Values of $p$ and $p_r$ are calculated based on the use of the extrapolated and the exact solutions, respectively (Section 2.1.1).

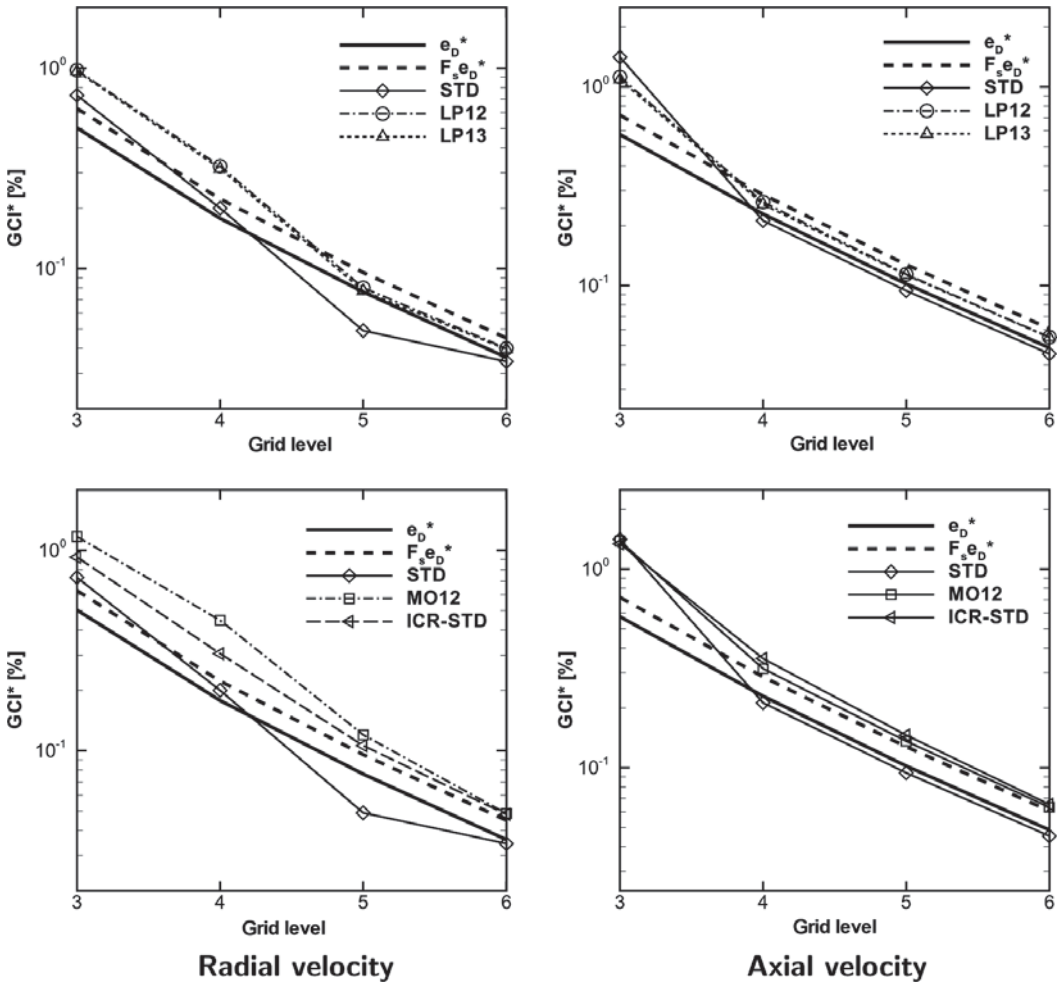


**Figure 4.** Case A. Manufactured solution. First-order in time discretization (1OT). Estimates of the GCI* and comparison with the exact discretizaton error ($e_D^*$).

to provide conservative estimates of the GCI*. Figure 4 shows that the GCI* underestimates the exact discretization error in five of the eight plotted values, including the four values obtained on the two finest grid levels. The highest underconservative deviation of the estimated $e_D$ from the exact value has been obtained for $v_r$ on grid level m5t5, where a discrepancy of approximately 50% is observed. Contrarily, methods LP12, LP13, and MO12 report conservative estimates of the GCI* in all solutions, noticeably overpredicting the discretization error in the coarsest grid level, and becoming more accurate as the grid is refined. Among these methods, MO12 also provides conservative estimates of $e_D^*$. Consequently, a value of $F_s = 1.0$ leads to more accurate results, without the loss of the required conservativeness. The two remaining SCR methods, LP23 and MO23, show a trend toward underconservative and fairly inaccurate results as the grid is refined. In fact, this is a predictable behavior, as first-order terms gain weight as the grid is refined, while MO23 simply neglects these terms, and LP23 assumes at least second-order convergence. Method MO23, however, still reports conservative and reasonably accurate estimates in the

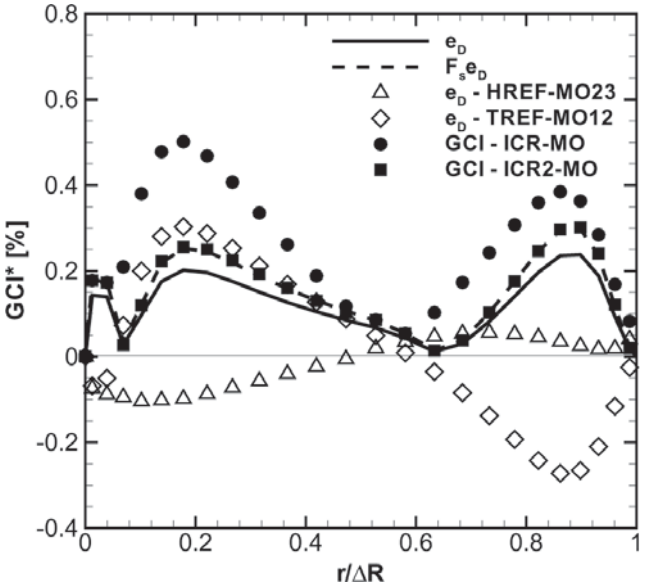


**Figure 5.** Case A. Manufactured solution. First-order in time discretization (1OT). Grid level 5. Local value of $e_D^*$ and GCI* corresponding to the axial velocity component at time instant $t/t_f = 0.75$ and section $z/2\pi = 0.42$. Legend: ($e_D$-HREF-MO23, $e_D$-TREF-MO12) $e_D$ values from HREF based on MO23, and from TREF studies based on MO12; (GCI-ICR-MO, GCI-ICR2-MO) GCI values from Eqs. (18) and (23), respectively.

coarsest grid level, where the weight of the first-order terms is lower, and method MO12 substantially overpredicts the error.

The results reported from the ICR-STD method display a similar trend to that of the MO12 method. Both methods provide conservative estimates of the GCI*, overly conservative on the coarsest grids and fairly accurate on the finest levels. The conservative behavior of the ICR-STD method can be attributed to the way that Eq. (18) sums the space and time discretization errors to evaluate the overall GCI. This point is further illustrated in Figure 5. This figure displays different profiles of local values of $e_D$ and the GCI obtained for $v_z$ at time instant $t/t_f = 0.75$ and section $z/2\pi = 0.42$. Here, to obtain continuous profiles of these estimators, the MO23 and MO12 methods have been respectively applied on the space and time directions. It can be observed that HREF and TREF studies have provided in this case estimates of the local $e_D$ of different sign on most points of the section. In such cases, the errors associated with the discretization on both coordinates partly cancels. However, this effect is not reproduced by Roache's equation (18), as the absolute-value operator is independently applied to $e_{D,s}(\mathbf{x}, t)$ and $e_{D,t}(\mathbf{x}, t)$. Consequently, Eq. (18) tends to provide conservative estimates of the GCI, as can be observed in the plot. Alternatively to the use of Eq. (18), the GCI could be evaluated from

$$\mathrm{GCI}(\mathbf{x}, t) = F_s |e_{D,s}(\mathbf{x}, t) + e_{D,t}(\mathbf{x}, t)| \tag{23}$$

which allows errors cancellation by applying instead the absolute-value operator to the sum of errors. The results obtained from this expression are also plotted in

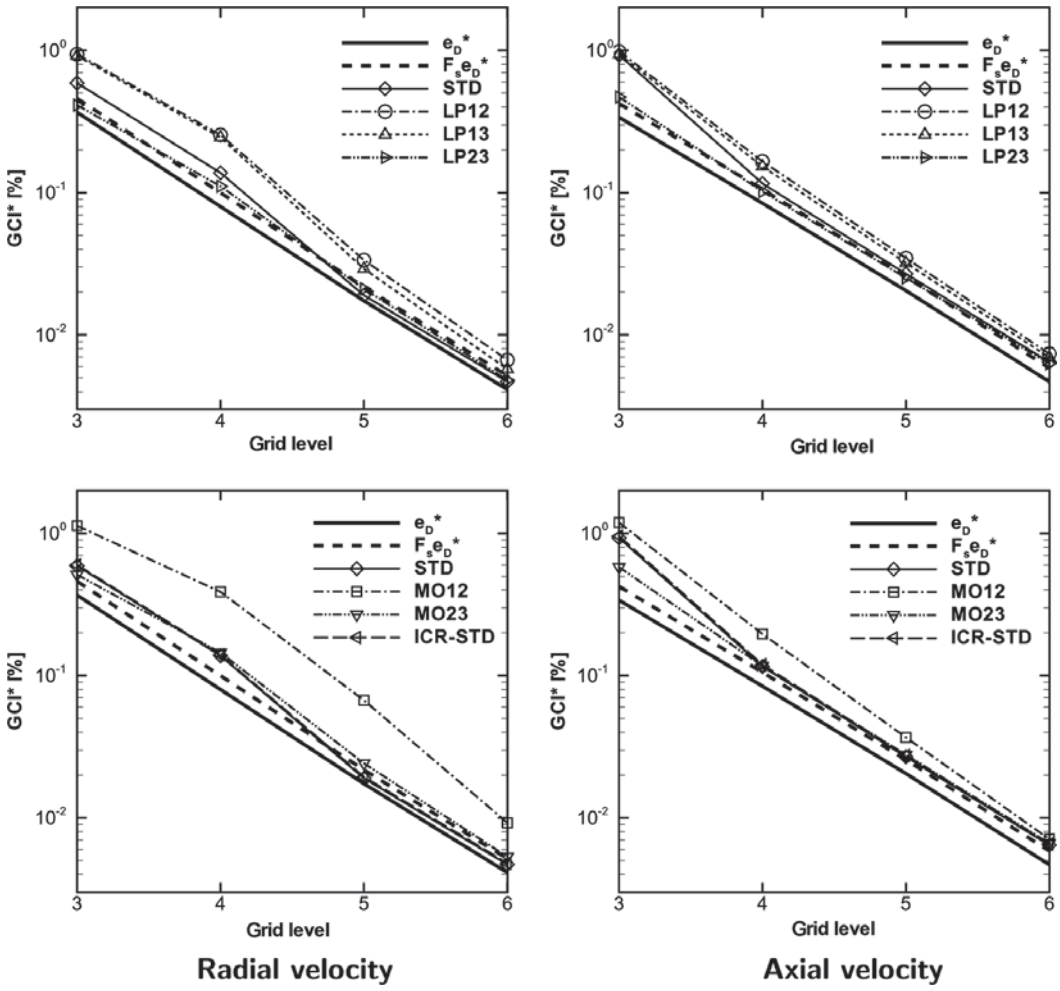


**Figure 6.** Case A. Manufactured solution. Second-order in time discretization (2OT). Estimates of the GCI* and comparison with exact the estimators of the discretization error ($e_D^*$).

Figure 5. It can be observed that Eq. (23) leads to substantially more accurate and still conservative enough results. Nevertheless, it must be borne in mind that, although this expression achieves greater accuracy in the estimation of the GCI, it also leads to less conservative results, increasing the risk of underconservative estimates of the GCI. At this point, a deeper investigation into the performance of Eq. (23) for verification purposes, and on the adequate value of $F_s$, is required. However, this task falls outside the scope of this study, and is left for future work.

The results obtained using the 2OT scheme differ substantially from those described above for 1OT. In this case, the postprocessing estimators reported in Table 3 show that the values of $p$ reported from SCR studies display a second-order trend, suggesting $v_z$ convergence closer to the asymptotic range. In addition, the ICR results suggest that the overall error is dominated mainly by the space discretization. Very similar values of $R_n$, $p$, and $\sigma_p$ have therefore been reported from both the SCR and HREF studies. Under these circumstances, the performance of the different methods is substantially different. Figure 6 shows that while, in general, methods

STD, MO23, and LP23 reported underconservative and inaccurate results for 1OT, these methods provide conservative estimates of the GCI* in all grid levels, and fairly accurate estimates on the finest one, for 2OT. Among these methods, MO23 also provided conservative estimates of the discretization error. Therefore, $F_s = 1$ leads to a narrower error band, which still contains the exact value of $e_D^*$. The ICR-STD method provided similar results to the STD method, as the error is dominated mostly by the space discretization. Contrarily, the LP12, LP13, and MO12, methods though always on the conservative side, reported less accurate estimates of $e_D^*$. These estimates are particularly inaccurate for $v_r$, as solutions seem to be converging farther from the asymptotic range. Contrarily, $v_z$ seems to approach the second-order asymptotic convergence range as the grid is refined. Under these conditions, estimates from all methods also become more accurate on the finest grids, therefore reducing the discrepancies among them. A maximum discrepancy of 17% is observed in the finest grid level, where the lowest value of $\sigma_p$ of all cases is also reported.

These results highlight that the formal order of accuracy of the discretization method is not sufficient information to select the most adequate limits of $p$ to be used in the LP methods, or error terms to be considered in the MO methods. Additional information on how the solution is converging on the grid sizes being used is therefore also required. Such information can be provided by the global observed $p$. However, the limitations of this estimator must be borne in mind in cases of mixed-order convergence. Such limitations can be partially overcome by the information obtained from HREF and TREF studies in those cases where the mixed-order convergence is due to the different-order convergence of the space and time discretization errors.

### 5.2. Case B

The postprocessing estimators of the observed order of accuracy obtained from SCR studies for both 1OT and 2OT schemes are reported in Table 4. The piston velocity $V_P$ has been used for normalization of the grid convergence index GCI*. Values of $R_n$ higher than 70% have been obtained in all cases, and higher than 80% on the finest grid levels. Values of $p$ reported from SCR studies show nonasymptotic error convergence in both the 1OT and the 2OT cases. ICR studies reveal

**Table 4.** Case B: incompressible flow on a piston–cylinder assembly, Richardson nodes, global $p$, and $\sigma_p$ obtained from SCR studies

| | 1OT | | | | | | 2OT | | | | | |
|---|---|---|---|---|---|---|---|---|---|---|---|---|
| | Radial velocity | | | Axial velocity | | | Radial velocity | | | Axial velocity | | |
| Grid triplet | $R_n$ (%) | $p$ | $\sigma_p$ | $R_n$ (%) | $p$ | $\sigma_p$ | $R_n$ (%) | $p$ | $\sigma_p$ | $R_n$ (%) | $p$ | $\sigma_p$ |
| 1/2/3 | 72 | 1.0 | 1.7 | 80 | 1.2 | 1.5 | 72 | 1.0 | 1.8 | 79 | 1.2 | 1.6 |
| 2/3/4 | 74 | 1.6 | 1.7 | 71 | 1.9 | 1.6 | 72 | 1.7 | 1.9 | 70 | 2.1 | 1.7 |
| 3/4/5 | 84 | 1.3 | 1.4 | 87 | 1.6 | 1.4 | 82 | 1.5 | 1.6 | 84 | 1.7 | 1.5 |
| 4/5/6 | 86 | 1.6 | 1.3 | 83 | 1.6 | 1.3 | 82 | 1.7 | 1.5 | 80 | 1.7 | 1.4 |

that such behavior is at least partially caused by the space discretization, which also converges nonasymptotically and has a similar or greater weight than the time discretization in all the solutions. Additionally, these results reported high values of $\sigma_p$ for all cases. Under such conditions of nonasymptotic error convergence, large discrepancies are observed among the estimates provided by the different methods.

In the 1OT case, ICR studies suggest that the total discretization error tends to be controlled by both the space and time discretizations as the grid is refined, with TREF studies showing first-order convergence with low values of $\sigma_p$. It therefore seems reasonable to exclude methods MO23 and LP23 as adequate estimators of the GCI, as first-order error terms are known to have a significant weight in the total discretization error. As illustrated for $v_z$ in Figure 7, results have shown that MO12 reports again the most conservative behavior among all methods. STD, on the other hand, provided less conservative estimates of the GCI* in all grid levels but the coarsest one. As shown in Figure 7, the maximum discrepancy between the two methods is reported for $v_z$ on grid level m4t4, where the GCI* provided by MO12 almost doubles the value provided by STD. These results, in line with those reported for Case A with 1OT, highlight the risk of STD underpredicting the GCI even in cases with a high number of Richardson nodes and where the observed $p$ lies within the expected limits. Method LP12 reported very similar results to LP13, providing estimates of the GCI up 44% higher than STD. Finally, ICR-STD behaved very similar to the STD method on the coarsest grid levels, tending to provide more conservative estimates of the GCI as the grid is refined and, as suggested by ICR studies, both the space and time discretizations have a similar weight on the overall error. A maximum difference with the STD method of about a 33% is observed for $v_z$ on the finest grid level.

In the 2OT case, ICR studies reveal that the total discretization error is basically controlled by the space discretization. Consequently, methods MO23 and

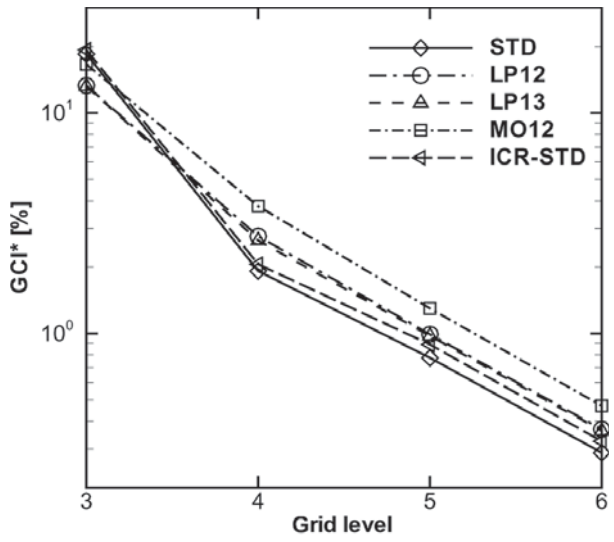


**Figure 7.** Case B. Incompressible flow on a piston–cylinder assembly. First-order in time discretization (1OT). Axial velocity component. Estimation of the GCI*.

LP23 cannot be excluded as adequate techniques for the estimation of the GCI, since no clear evidence of first-order terms controlling the discretization error exists. Although not shown, similar to the 1OT case, method MO12 provided the most conservative estimates of the GCI in all grid levels except for $v_z$ on the coarsest grid. This method provided estimates of the error ranging from 165% to 265% higher than LP23, which provided less conservative values of the GCI in all grid levels.

### 5.3. Case C

The estimators of the observed order of accuracy obtained from SCR studies are reported in Table 5. The GCI values of both velocity and temperature presented in Figures 8 and 9 have been normalized in terms of the maximum piston velocity and the initial gas temperature, respectively. SCR studies report high values of $R_n$, especially for the finest grid levels, where $R_n > 90\%$ is observed. HREF studies suggest, on the one hand, space discretization tending toward second-order convergence for both velocity components, and second-order convergence for the temperature. On the other hand, TREF studies shows a clear first- and second-order convergence for schemes 1OT and 2OT, respectively. In all cases, TREF studies reported very low values of $\sigma_p$.

For the 1OT scheme, ICR studies reveal discretization error being controlled by both the space and time discretizations for both velocity components, with time discretization tending to dominate the error on the finest mesh levels for $v_z$. Consequently, as first-order terms from the time discretization cannot be neglected, methods LP23 and MO23 have not been considered. In line with the results obtained previously in cases of mixed-order convergence, although not shown, the results obtained for $v_r$ from the remaining methods reveal noticeable discrepancies between the GCI values provided by MO12 and the other methods. The maximum discrepancy is observed between methods MO12 and both STD and ICR on grid level m5t5, where MO12 provides a value of the GCI about 95% higher. In the case of $v_r$, as shown in Figure 8, these discrepancies become substantially smaller on the finest grid levels, as the time discretization tends to dominate the overall discretization error. Additionally, lower values of $\sigma_p$ have also been reported. For this variable,

**Table 5.** Case C: Gas spring, Richardson nodes, global $p$, and $\sigma_p$ obtained from SCR studies

| | Radial velocity | | | Axial velocity | | | Temperature | | |
|---|---|---|---|---|---|---|---|---|---|
| Grid triplet | $R_n$ (%) | $p$ | $\sigma_p$ | $R_n$ (%) | $p$ | $\sigma_p$ | $R_n$ (%) | $p$ | $\sigma_p$ |
| | | | | 1OT | | | | | |
| 1/2/3 | 69 | 1.3 | 1.7 | 85 | 1.0 | 1.4 | 84 | 1.5 | 1.4 |
| 2/3/4 | 80 | 1.2 | 1.4 | 90 | 1.0 | 1.1 | 92 | 1.4 | 1.2 |
| 3/4/5 | 90 | 1.5 | 1.2 | 95 | 1.1 | 0.8 | 95 | 1.2 | 1.0 |
| 4/5/6 | 93 | 1.5 | 1.1 | 96 | 1.1 | 0.7 | 96 | 1.1 | 0.9 |
| | | | | 2OT | | | | | |
| 1/2/3 | 69 | 1.5 | 1.6 | 83 | 1.7 | 1.8 | 79 | 2.2 | 1.6 |
| 2/3/4 | 82 | 1.5 | 1.4 | 89 | 1.8 | 1.3 | 92 | 2.1 | 1.3 |
| 3/4/5 | 94 | 1.9 | 1.0 | 94 | 1.9 | 0.8 | 96 | 2.1 | 0.9 |
| 4/5/6 | 96 | 2.0 | 0.8 | 97 | 1.9 | 0.7 | 98 | 2.1 | 0.6 |

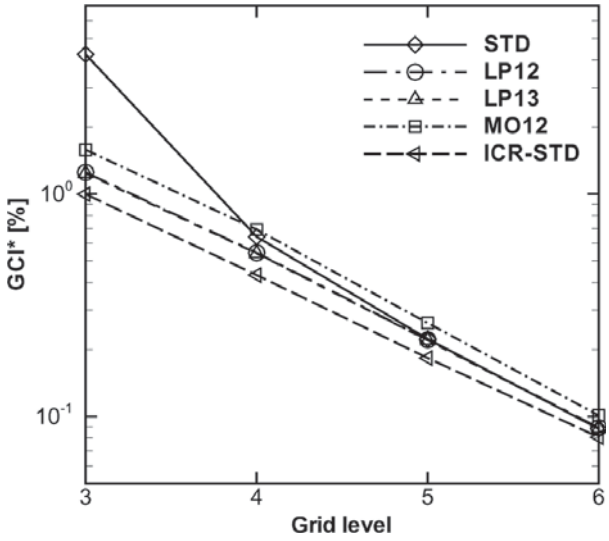


**Figure 8.** Case C. Gas spring. Axial velocity. First-order in time discretization (1OT). Estimation of the GCI*.

MO12 predicts a value of the GCI 25% higher than ICR-STD in the finest grid level, which shows less conservative behavior on all grid levels, and, contrary to what was observed in previous cases, provides results less conservative than the STD method.

Although results for the 2OT scheme are not provided, ICR studies have shown that the overall error is clearly controlled by the space discretization for both velocity components, with HREF studies suggesting values of the GCI* 50 to 400 times higher than TREF. Despite the observed second-order trend for both variables, the high discrepancies reported among all methods also suggest mixed-order

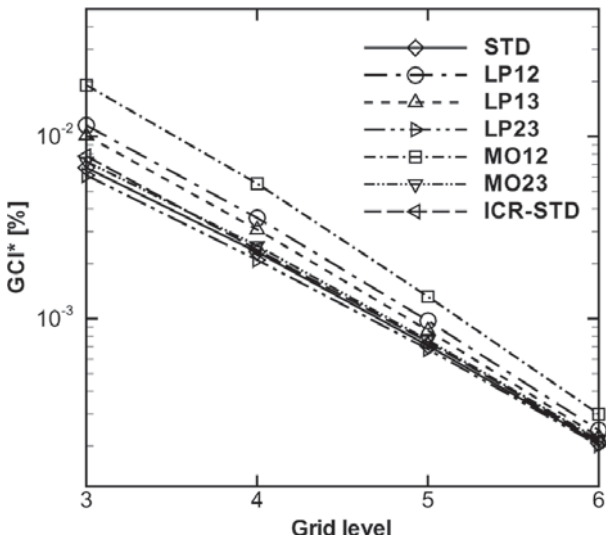


**Figure 9.** Case C. Gas spring. Temperature. Second-order in time discretization (2OT). Estimation of the GCI*.

convergence of the space discretization. Under these conditions, the most conservative results are, in general, provided by MO12, which reports values more than 200% higher than those obtained from LP23, which provides less conservative estimations of the GCI in all grid levels.

Finally, ICR studies conducted for temperature suggest error tending to be controlled by the time discretization for 1OT and the space discretization for 2OT. In both cases, estimations of the $GCI^*$ obtained from both HREF and TREF studies, although not provided, suggested that the errors associated with the dominating discretizations are about 20 times higher on the finest grid level. As in previous cases, methods LP23 and MO23 have been ruled out for the 1OT. Results revealed that although noticeable discrepancies are observed on the coarsest grid levels, all methods tend to provide similar results as the grid is refined. This behavior has been illustrated in Figure 9 for the 2OT scheme. These results suggest that the error approaches the asymptotic range of convergence on the finest grid level and, consequently, the accuracy of all methods also increases with grid refinement.



## 6. CONCLUSIONS

This work has addressed the verification of multidimensional and transient numerical solutions based on grid refinement studies and the Richardson extrapolation techniques. Different verification methods based on alternative extrapolation strategies, and on both the simultaneous and the independent refinement of coordinates, have been investigated. Extrapolation strategies studied encompass the generalized Richardson extrapolation (GRE) based on both the local and the global observed order of convergence, and the mixed-order Richardson extrapolation (MORE). Discussion has been included of the performance of each method for the verification of a manufactured solution (MMS), and both incompressible and compressible flows on different piston–cylinder configurations.

The results reveal that none of the studied methods performed equally satisfactorily in all tested cases. The MMS case showed that while method STD provided conservative estimates of the GCI in all grid levels and fairly accurate ones on the finest one for method 2OT, it failed to provide conservative estimates of the GCI in five of eight values assessed for the 1OT case, despite the high percentage of Richardson nodes and that values of $p$ within the expected limits were obtained.

In general, MO12 showed the most conservative behavior of all the methods investigated in all tested cases. This method always provided conservative predictions of the discretization error in Case A, where the exact error was available by means of a manufactured solution. Therefore, a value of $F_s = 1.0$ would have led in this case to more accurate results, without the loss of the required conservativeness of the method. Lacking the exact solution for Cases B and C, it cannot be confirmed whether this statement also holds for these cases. However, the more conservative estimates of the GCI provided by method MO12, when compared with the results obtained from other methods, seem to suggest that MO12 might require values of $F_s$ less conservative than those required by other methods. This point, however, requires further evidence and will be the subject of future work.

It has also been highlighted that the formal order of accuracy of the discretization method is not sufficient information to select the most adequate limits of $p$ to be used in the LP methods, or the error terms to be considered in the MO methods. Additional information on how the solution is converging is therefore also required. Such information can in some cases be provided by the global observed $p$. However, the limitations of this estimator in cases of mixed-order convergence must be borne in mind. These limitations can be partially overcome by the information obtained from ICR studies in cases of mixed-order convergence originated by the different-order discretization of the space and time coordinates. An alternative expression to that proposed by Roache for the estimation of the overall value of the GCI in ICR studies has also been briefly discussed and assessed. Despite the satisfactory results presented, a deeper investigation into its performance for verification purposes and into the adequate value of $F_s$ is required.

Finally, different cases have been identified where the estimated value of the global $p$ systematically suggests second-order convergence in consecutive grid levels, which might be interpreted as convergence approaching the second-order asymptotic limit. However, the high discrepancies obtained in some cases among solutions provided from different methods, e.g., MO12 and MO23, suggest that solution might be actually converging far from second-order asymptotic range. The correct use of $p$ as a representative indicator of the real solution convergence on which the most adequate verification techniques can be selected, and its dependence on the observed value of $\sigma_p$, therefore needs to be investigated further.

## REFERENCES

1. W. L. Oberkamp and T. G. Trucano, Verification and Validation in Computational Fluid Dynamics, *Tech. Rep.*, Sandia National Laboratories, Albuquerque, NM, 2002.
2. F. G. Blottner, Accurate Navier-Stokes Results for the Hypersonic Flow over a Spherical, Nosetip, *AIAA J. Spacecraft Rockets*, vol. 27, pp. 113–122, 1990.
3. L. Eça and M. Hoekstra, An Evaluation of Verification Procedures for CFD Applications, in *Proc. 24th Symp. on Naval Hydrodynamics*, Fukuoka, Japan, 2002.
4. I. Celik and G. Hu, Single Grid Error Estimation Using Error Transport Equation, *J. Fluids Eng.*, vol. 126, no. 5, pp. 778–790, 2004.
5. P. J. Roache, *Verification and Validation in Computational Science and Engineering*, Hermosa, Albuquerque, NM, 1998.
6. J. E. Jaramillo, C. D. Pérez-Segarra, I. Rodríguez, and A. Oliva, Numerical Study of Plane and Round Impinging Jets Using RANS Models, *Numer. Heat Transfer B*, vol. 54, pp. 213–237, 2008.
7. F. Stern, R. V. Wilson, H. W. Coleman, and E. G. Paterson, Comprehensive Approach to Verification and Validation of CFD Simulations—Part 1: Methodology and Procedures, *J. Fluids Eng.*, vol. 123, pp. 793–802, 2001.
8. P. H. Gaskell and A. K. C. Lau, Curvature-Compensed Convective Transport: SMART, a New Boundedness-Preserving Transport Algorithm, *Int. J. Numer. Meth. Fluids*, vol. 8, pp. 617–641, 1988.
9. I. Celik and O. Karatekin, Numerical Experiments on Application of Richardson Extrapolation with Nonuniform Grids, *J. Fluids Eng.*, vol. 119, pp. 584–590, 1997.
10. J. Cadafalch, C. D. Pérez-Segarra, R. Cònsul, and A. Oliva, Verification of Finite Volume Computations on Steady State Fluid Flow and Heat Transfer, *J. Fluids Eng.*, vol. 124, pp. 11–21, 2002.

11. L. F. Richardson, On the Approximate Arithmetical Solution by Finite Differences of Physical Problems Involving Differential Equations, with an Application to the Stresses in a Masonry Dam, *Proc. Roy. Soc. A*, vol. 83, pp. 335–336, 1910.
12. L. F. Richardson and J. A. Gaunt, The Deferred Approach to the Limit. Part I. Single Lattice. Part II. Interpenetrating Lattices, *Proc. Roy. Soc. A*, vol. 226, pp. 299–361, 1927.
13. C. J. Roy, Grid Convergence Error Analysis for Mixed-Order Numerical Schemes, *AIAA J.*, vol. 41, pp. 595–604, 2003.
14. C. J. Roy, M. A. Mc Wherter-Payne, and W. L. Oberkampf, Verification and Validation for Laminar Hypersonic Flowfields, Part 1: Verification, *AIAA J.*, vol. 41, pp. 1934–1943, 2003.
15. L. Eça and M. Hoekstra, On the Grid Sensitivity of the Wall Boundary Condition of the $k-\omega$ Turbulence Model, *J. Fluids Eng.*, vol. 126, pp. 900–910, 2004.
16. M. S. Darwish and F. Moukalled, Normalized Variable and Space Formulation Methodology for High-Resolution Schemes, *Numer. Heat Transfer B*, vol. 26, pp. 79–96, 1994.
17. P. J. Roache, Code Verification by the Method of Manufactured Solutions, *J. Fluids Eng.*, vol. 124, pp. 4–10, 2002.
18. J. P. Van Doormal and G. D. Raithby, Enhancements of the Simple Method for Predicting Incompressible Fluid Flows, *Numer. Heat Transfer*, vol. 7, pp. 147–163, 1984.
19. C. D. Pérez-Segarra, A. Oliva, M. Costa, and F. Escanes, Numerical Experiments in Turbulent Natural and Mixed Convection in Internal Flows, *Int. J. Numer. Meth. Heat Fluid Flow*, vol. 5, pp. 13–33, 1995.
20. F. Durst, T. Maxworthy, and J. C. F. Pereira, Piston-Driven, Unsteady Separation at a Sudden Expansion in a Tube: Flow Visualization and LDA Measurements, *Phys. Fluids*, vol. 1, pp. 1249–1260, 1989.
21. H. Ströll, F. Durst, M. Peric, J. C. F. Pereira, and G. Scheuerer, Study of Laminar, Unsteady Piston-Cylinder Flow, *J. Fluids Eng.*, vol. 115, pp. 687–693, 1993.